AD-A105 704 ARMY ARMAMENT RESEARCH AND DEVELOPMENT COMMAND DOVER--ETC F/G 20/11
SHOCK FRONT RISE TIME IN WATER.(U)
OCT 81 P HARRIS, H PRESLES
UNCLASSIFIED ARLCD-TR-81032 SBIE-AD-E400 719 NL

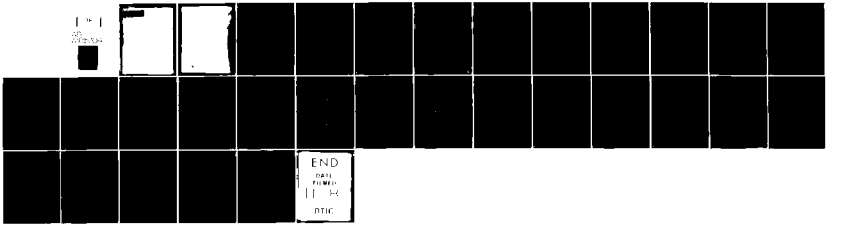

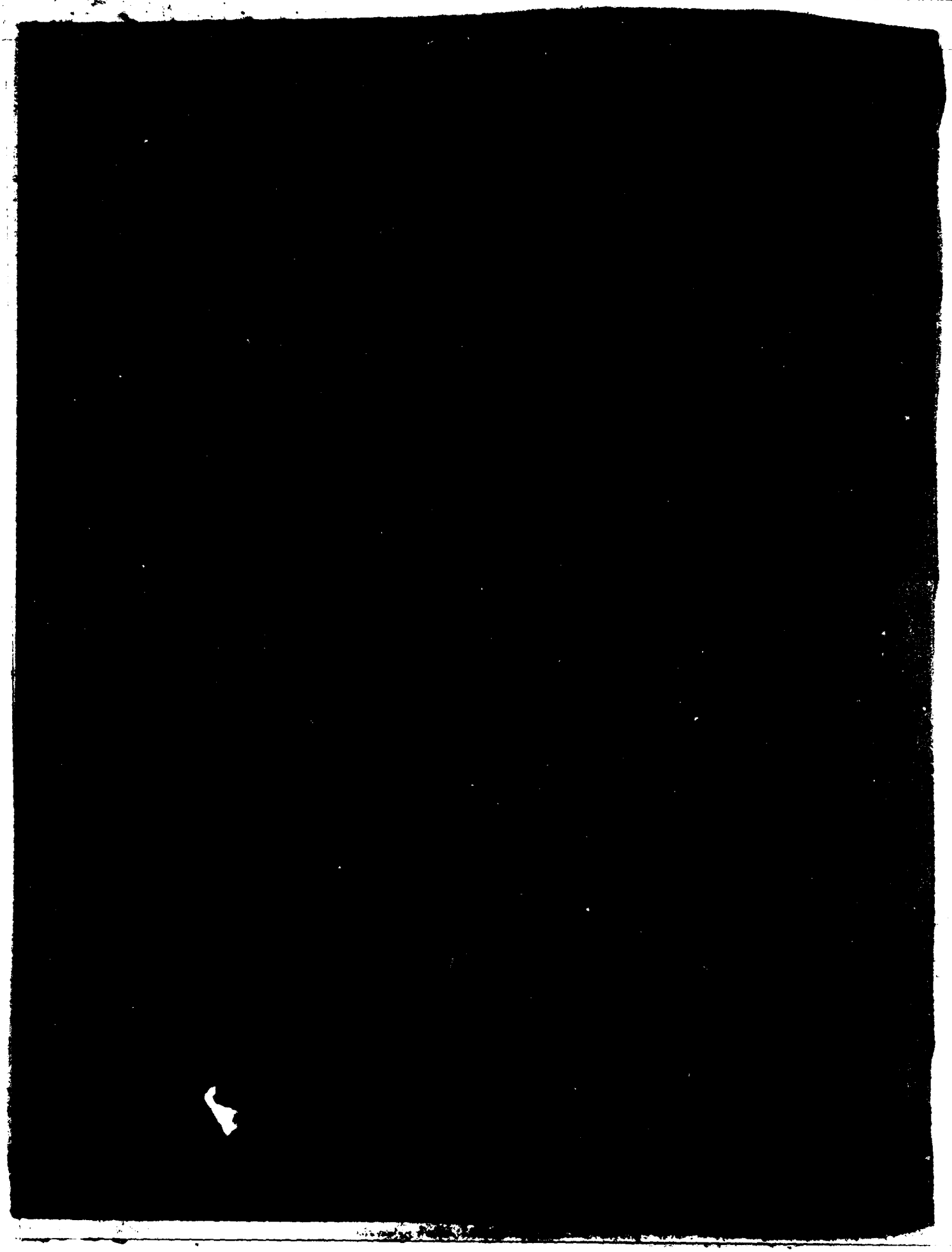

UNCLASSIFIED

SECURITY CLASSIFICATION OF THIS PAGE (When Date Entered)

REPORT DOCUMENTATION PAGE		READ INSTRUCTIONS BEFORE COMPLETING FORM
1. REPORT NUMBER Technical Report ARLCD-TR-81032	2. GOVT ACCESSION NO. AD-A105	3. RECIPIENT'S CATALOG NUMBER 704
4. TITLE (and Subtitle) SHOCK FRONT RISE TIME IN WATER		5. TYPE OF REPORT & PERIOD COVERED Program Status Report to October 1981 6. PERFORMING ORG. REPORT NUMBER
7. AUTHOR(s) Paul Harris, ARRADCOM Henri-Noel Presles, University of Portiers, Portiers, France		8. CONTRACT OR GRANT NUMBER(s)
9. PERFORMING ORGANIZATION NAME AND ADDRESS ARRADCOM, Dover, NJ 07801 University of Poitiers, Poitiers, France		10. PROGRAM ELEMENT, PROJECT, TASK AREA & WORK UNIT NUMBERS 1L161101A91A
11. CONTROLLING OFFICE NAME AND ADDRESS ARRADCOM, TSD STINFO Div (DRDAR-TSS) Dover, NJ 07801		12. REPORT DATE October 1981 13. NUMBER OF PAGES 32
14. MONITORING AGENCY NAME & ADDRESS(if different from Controlling Office)		15. SECURITY CLASS. (of this report) Unclassified 15a. DECLASSIFICATION/DOWNGRADING SCHEDULE

16. DISTRIBUTION STATEMENT (of this Report)

Approved for public release; distribution unlimited.

17. DISTRIBUTION STATEMENT (of the abstract entered in Block 20, if different from Report)

18. SUPPLEMENTARY NOTES

19. KEY WORDS (Continue on reverse side if necessary and identify by block number)

shock wave rise time
shock polarization

20. ABSTRACT (Continue on reverse side if necessary and identify by block number)

A review is made of the present status of the experimental-theoretical program for the evaluation of the shock front thickness in water, and the results of recently performed hyperbolic tangent shock front structure calculations are presented. The hyperbolic tangent results, when compared with experimental data, predict a shock front thickness upper limit of 6.2×10^{-6} cm at 5.8 kbar.

contd

DD FORM 1 JAN 73 1473 EDITION OF 1 NOV 65 IS OBSOLETE

Unclassified

SECURITY CLASSIFICATION OF THIS PAGE (When Date Entered)

20. ABSTRACT -contd

Experiments and theory planned for the near future are outlined. These experiments will involve shock front optical reflectivity and shock polarization voltage measurements. Some preliminary theory corresponding to these planned experiments is presented. In particular, a net electric dipole alignment calculation is presented which predicts approximately 5 mv across a 50-ohm load at 15 kbars.

The anomalously large Soviet shock viscosity results are considered (without resolution of the question), and the possibility of significant hydrogen bond breaking at shock pressures above 5.8 kbars is discussed.

CONTENTS

FIGURES

ACKNOWLEDGEMENTS

The authors appreciate the assistance of H. Simonnet (University of Poitiers), for conducting the experiments, and of R. Schutz (ARRADCOM) for bringing the existence of DCADRE to our attention and for implementing the program.

The authors acknowledge the helpful discussions of F. H. Stillinger (Bell Telephone Laboratories) and R. A. Graham (Sandia National Laboratories). The helpful correspondence of S. D. Hamann (CSIRO, Australia) is also acknowledged.

The authors are grateful to the U.S. Army Research and Standardization Group (UK) for financial support of travel between ARRADCOM and the University of Poitiers.

INTRODUCTION

This report discusses the results of the first set of experiments and corresponding theory relating to the evaluation of the rise time of a shock front in water. This report also discusses the planned second stage of experimentation and corresponding theory wherein outstanding questions are to be addressed, and where a preliminary evaluation of the shock front rise in the explosive liquid, nitromethane, is to be made.

The primary reason for choosing liquid nitromethane is simple; it remains transparent at shock pressures below those necessary for shock initiation of detonation. Furthermore, experiments have demonstrated a shock-generated voltage of approximately 0.1 volt (50 Ω termination) in liquid nitromethane at 50 kbar (ref 1). If that 0.1-volt potential drop were to exist entirely across a small shock front thickness (of the order of tens of molecular diameters), an electrical breakdown mechanism would exist for bond breaking and consequent chemistry.

THE SHOCK FRONT THICKNESS AT 5.8 kbar

Two recent publications (refs 2 and 3) have outlined the experimental program and detailed the theory leading to the results shown in figure 1. This figure indicates that a combination of $\beta \leq 0.2$ and $(\Delta n)_f \geq 5.26 \times 10^{-2}$ is necessary for agreement between theory and experiment.

The calculations illustrated in figure 1 were carried out with a constant gradient,

$$\left(\text{i.e. } \frac{\partial n}{\partial x} = \frac{(\Delta n)_f}{L} = \text{constant, } n = \text{index of refraction, and } L = \text{shock front thickness}\right)$$

shock front model. $\beta \equiv (Ln_o/\lambda_o)$, and $(\Delta n)_f$ is the total change in index of refraction across the shock front. n_o is the unshocked state index, and λ_o is optical wavelength in vacuum.

For $\lambda_o = 5145$ Å and $n_o = 1.33$, the result $\beta \leq 0.2$ gives $L \leq 623$ Å, or approximately 215 molecular lengths for an oxygen-oxygen distance of 2.9 Å. $(\Delta n)_f = 5.26 \times 10^{-2}$ corresponds to the expected index of refraction change at 5.8 kbar from equation-of-state (EOS) data (ref 3).

With the constant gradient model, the reflectivity R can be put in the form

$$R = \sin^2 \left[1/2 \int_o^{m_f} (1 \pm \tan^2\theta) \cos \left\{ \frac{2\pi}{m_f} \left[(m+1)^2 \left\{ 1 - \left(\frac{\sin\theta_o}{m+1} \right)^2 \right\}^{1/2} + \right. \right. \right.$$

$$\left. \left. \left. - \cos\theta_o - (\sin^2\theta_o) \ln \frac{(m+1)\left(1 + \left[1 - \left(\frac{\sin\theta_o}{m+1}\right)^2\right]^{1/2}\right)}{1 + \cos\theta_o} \right\} \right] dm, \qquad (1)$$

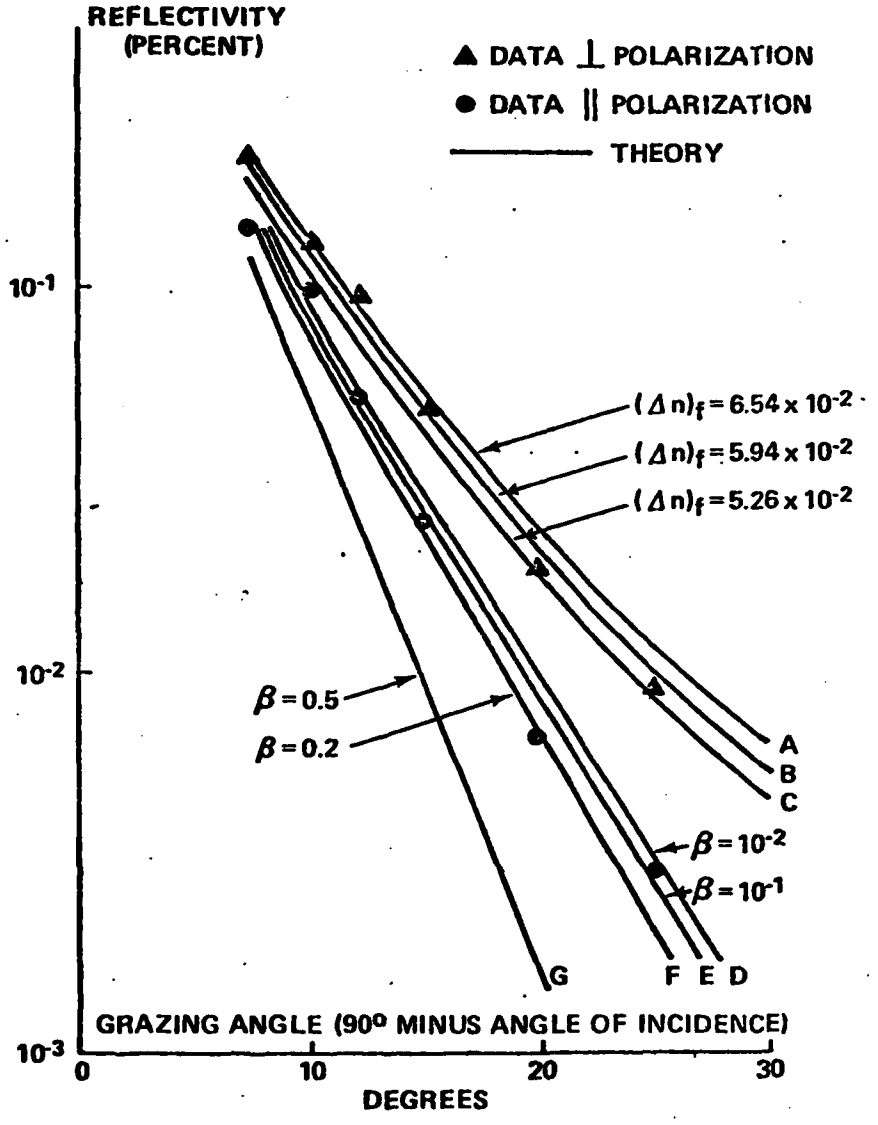

Figure 1. Theory and experimental data for shock front reflectivity at 5.8 kbar in water. Curves A, B, and C are for ⊥ optical polarization and $\beta = (n_o L/\lambda_o) = 0.1$. Curves D through G are for ∥ optical polarization and $(\Delta n)_f = 5.26 \times 10^{-2}$. Constant gradient model calculations.

$$1 - \tan^2\theta = \frac{(m+1)^2 - 2\sin^2\theta_o}{(m+1)^2 - \sin^2\theta_o}, \tag{2a}$$

$$1 + \tan^2\theta = \frac{(m+1)^2}{(m+1)^2 - \sin^2\theta_o}. \tag{2b}$$

In equation 1, the plus-and-minus signs refer to incident beam optical polarization perpendicular and parallel to the plane of incidence, respectively. θ_o is the angle of incidence in the unshocked medium, and $m \equiv (\Delta n)/n_o$. The argument of the cosine term in equation 1 represents the effect of the optical phase difference (at the reflectivity measuring photo-diode) due to reflection from different layers within the shock front.

While the constant gradient model is simple, both conceptually and algebraically, it is not realistic; the foot and plateau discontinuities in $\frac{\partial n}{\partial x}$ (equivalent to discontinuities in $\frac{\partial \rho}{\partial x}$, ρ = mass density) would not be expected to occur in the presence of viscosity. A more realistic (but not necessarily correct) shock front model is the hyperbolic tangent model characteristic of weak shock propagation in gases (ref 4). Indeed, Cowan and Hornig (ref 5) have employed the hyperbolic tangent model in evaluating shock front reflectivity measurements in gases.

Writing the hyperbolic tangent model as

$$n - n_o = \frac{(\Delta n)_f}{1 + e^{-4x/L}} \tag{3}$$

gives for the reflectivity

$$R = \sin^2 \left[1/2 \int_o^{m_f} (1 \pm \tan^2\theta) \cos \frac{\pi L}{\lambda_o} \int_o^{m} \frac{m_f (1 + m')n_o}{m'(m_f - m')} \times \right.$$

$$\left. \times \left[1 - \left(\frac{\sin\theta_o}{1 + m'} \right)^2 \right]^{1/2} dm' \right] dm. \qquad (4)$$

The difference between equations 1 and 4 is entirely due to phasing effects. The presence of the m' and $(m_f - m')$ terms in denominator of the cosine argument of equation 4 is representative of index-of-refraction changes spatially extending from $-\infty$ to $+\infty$.

Although algebraically complicated, equation 1 is easier to integrate numerically (by partitions) than is equation 4; singularities occur in the inner integral for the outer integral limits. If the mentioned singularities are treated via the cutoff procedure,

$$m' \equiv m_f \times 10^{-3} \quad \text{if} \quad m' < m_f \times 10^{-3}, \text{ and} \qquad (5)$$

$$(m_f - m') \equiv m_f \times 10^{-3} \quad \text{if} \quad (m_f - m') < m_f \times 10^{-3}, \qquad (6)$$

then the perpendicular polarization results illustrated in figure 2 are obtained via numerical integration techniques. The figure 2 results were obtained by using $(\Delta n)_f = 5.26 \times 10^{-2}$ and the "DCADRE" integration program[1] recursively. DCADRE uses a Romberg extrapolation routine.

Figure 2 shows that the hyperbolic tangent results are essentially the same as those obtained with the constant gradient model. The main differences between the two sets of results are:

1. In the hyperbolic tangent case, varying $\beta = Ln_o/\lambda_o$ from 0.2 to 10^{-3} no longer shifts the data across the range of experimental data (see the parallel polarization data and calculations of fig. 1).

2. The maximum reflectivity value (that obtained for $\beta = 10^{-3}$) just coincides with the lower edge of the data band.

---

[1]Copyrighted 1978 and commercially available from IMSL, Inc., 7500 Bellaire Blvd., Houston, TX 77036.

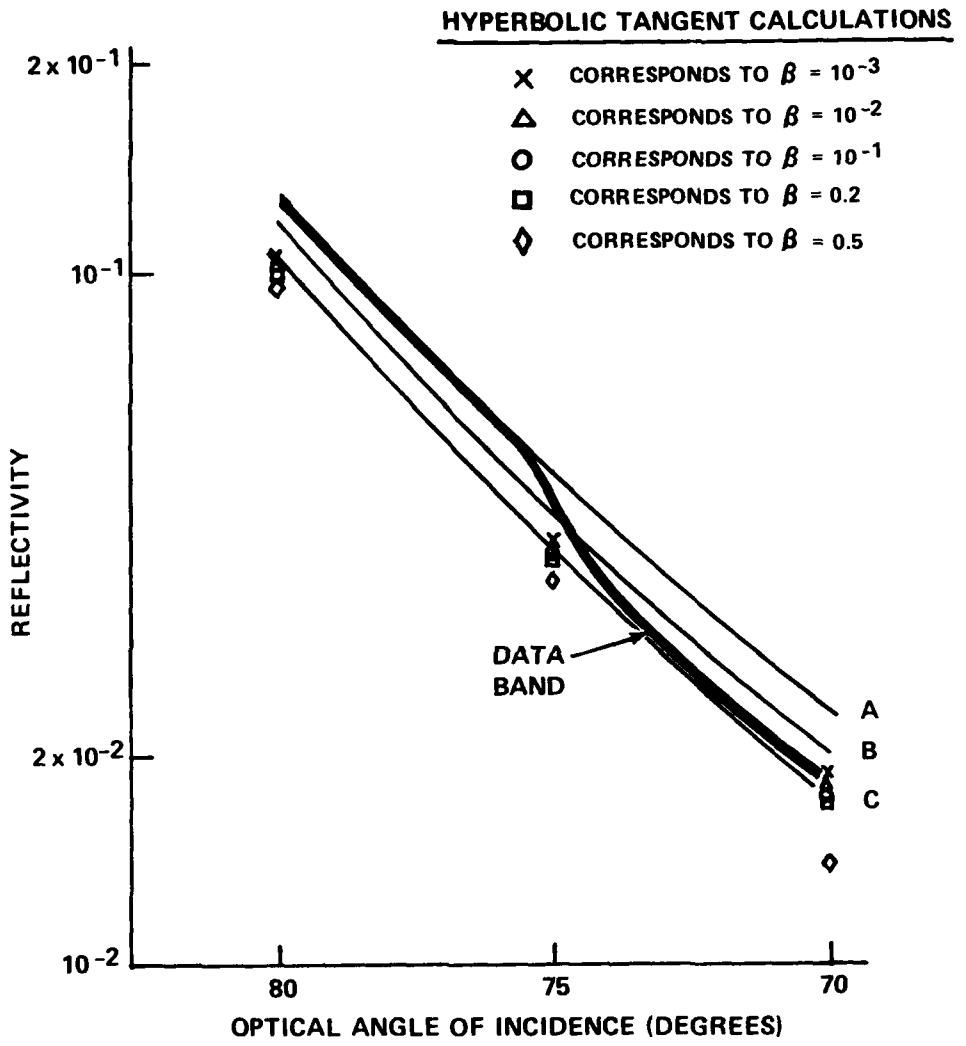

Figure 2. Hyperbolic tangent shock front calculations for perpendicular optical polarization at 5.8 kbar. Curves A, B, and C are constant gradient model results (as in fig. 1). All hyperbolic tangent results are for $(\Delta n)_f = 5.26 \times 10^{-2}$.

The implications of the hyperbolic tangent model are essentially the same as previously reported (ref 3) for the constant gradient model: first, a shock front thickness characterized by $\beta \leq 0.2$ (equivalently ≤ 215 molecular lengths) and second, the possible necessity of a non-equation-of-state (non-EOS) contribution to the final index-of-refraction change. Such a non-EOS contribution, if positive, would increase the calculated reflectivity for a given value of β.

For a given value of β and $(\Delta n)_f$, the hyperbolic tangent reflectivity will be less than the corresponding constant gradient model reflectivity (because Δn limbs which extend spatially from $-\infty$ to $+\infty$ introduce destructive optical interference). As β increases, the hyperbolic tangent destructive interference increases faster than is the case with the constant gradient model. It is precisely this optical interference effect which prevents the hyperbolic tangent reflectivity results from sweeping across the experimental data band as β is increased.

Thus, if anything, the hyperbolic tangent model results reinforce the possible necessity for a non-EOS contribution to (Δn). It must be admitted, however, that the necessity for introducing a non EOS contribution to (Δn) is not glaring, and a definitive conclusion with respect to the (Δn) origin awaits better experimental accuracy.

It is difficult to measure the dimensions of an object with a comparison scale (ruler) which is either much larger or much smaller than the object to be measured. It was hoped that if $L \ll \lambda_o$ was indeed true, the spatially extended (Δn) limbs associated with the hyperbolic tangent model would effectively yield a ruler and L value of comparable size. Such has not proved to be the case.

SHOCK FRONT THICKNESS PHYSICS

The question of shock front thickness has intrigued shock wave physicists for many years. While the thickness in a gas is well understood in terms of being a few collision mean free paths (refs 5 and 6), the thickness in a condensed medium has been a question of some controversy (e.g., the mean free path of what excitation?).

By utilizing computer molecular dynamics (CMD), techniques D. Tsai et al (refs 7 and 8) have, for many years, demonstrated results which are consistent with a rise time occurring over a few lattice parameters. While Tsai's results were initially for solids, other workers (refs 9 and 10) had reached similar conclusions for monatomic liquids. Indeed Tsai et al (ref 11) speculate that 5 to 10 lattice parameters (rise time) is a universal effect associated with an "'inertial effect' in a discrete system."

If one thinks of a liquid as being a very dense gas, and as such not containing any excitations characteristic of long range order, then the water molecules themselves must represent the only entities one would wish to consider from a mean-free path point of view. Five to ten lattice parameters (oxygen-oxygen

distances) correspond to $\beta \leq 10^{-2}$, a number not inconsistent with the results demonstrated in figures 1 and 2.

It should be noted, however, that to the extent that there is hydrogen bonding in liquid water (refs 12 and 13) there is the possibility that such hydrogen bonding will result in significant long range order and that the long range order could control the shock front rise time. At this point, the experimental-theoretical program described in this report is unable to decide the issue.

IMPLICATIONS

Normally this information would appear at or near the end of a report. In this case, however, the implications serve at least as a partial motivation for the following two sections covering the next set of theory and experiment.

A shock front thickness of less than 30 Å would have both basic and applied implications. The applied aspect pertains to the possibility of a new concept in the shock initiation of explosives, while the basic aspect concerns the possibility of a better understanding of the detailed molecular motions occurring within a shock front in a liquid (e.g., by validating the CMD approach).

As previously mentioned, one observes a potential 0.1-volt drop when liquid nitromethane is shocked to near, but less than, 50 kbars. If the shock front thickness in the liquid nitromethane is assumed to be 30 Å, and if the potential drop is assumed to occur only across that shock front thickness,[2] the result is an electric field, E_{SF}, within the shock front given by

$$E_{SF} = \frac{0.1 \quad \text{volts}}{3 \times 10^{-7} \text{ cm}} = 3 \times 10^{-5} \quad \frac{\text{volts}}{\text{cm}} \tag{7}$$

The value of E_{SF} given by equation 7 clearly approaches the magnitude necessary for electrical breakdown.

If electrical breakdown were to be recognized as synonymous with bond breaking, and bond breaking synonymous with the criteria for the onset of chemistry, then one would have a conceptually simple model with which to explain shock initiation of explosives -- a shock front thickness which decreases as pressure increases until electrical breakdown and chemistry are achieved.

---

[2]While it is well known that many liquids have an electrochemical "shock polarization" contribution (refs 14 and 15), perhaps a sufficient fraction of the 0.1 volt will appear across the shock front (due to the orientation of molecular dipoles) to make equation 7 essentially correct.

The two ingredients associated with the electrical breakdown concept are the shock-induced "polarization" voltage and the front thickness as a function of shock amplitude (pressure). These two ingredients serve as the basis for the next set of theory and experiments. The front thickness as a function of pressure will be pursued, as before, from a continuum[3] optical-mechanical point of view. The polarization voltage, however, in sofaras it involves the partial alignment of molecular electrical dipoles, is a molecular level calculation.

Our recent publications (refs 2 and 3) attempted to show a relationship between a 5.8 kbar shock front thickness upper limit of approximately 215 oxygen-oxygen distances and Soviet-reported anomalously high viscosity values of approximately 10^4 P in the 100-kbar region. Unfortunately, the hyperbolic tangent results illustrated in figure 2 maintain the previously reported shock front thickness upper limit (refs 2 and 3) and thus do not resolve the viscosity question. It is worth noting, however, that Hamann[4] (ref 17) casts doubt on the interpretation of some of those Soviet shock viscosity experiments and also doubts that some of the Soviet experiments have measured shock front (as distinct from behind the shock) viscosity as we had previously maintained (ref 3).

One possible explanation for the Soviet viscosity observations could be the breaking[5] of hydrogen bonds in the 100-kbar region. As hydrogen bonds result in a restoring force which acts to counter a net alignment of molecular dipoles (see the section on Shock Polarization), bond breaking should increase observed shock polarization voltage amplitudes for water. This explanation is consistent with the concept by Graham (ref 18) wherein bond breaking is claimed to be responsible for the observed shock polarizability of polymeric solids. Thus, the planned shock polarization experiments and their theoretical interpretation should be very pertinent to the question of Soviet-claimed viscosity values.

REFLECTIVITY VERSUS PRESSURE

The upcoming reflectivity-versus-pressure experiments will be analyzed, as was done previously, by using the constant gradient and hyperbolic tangent models for data at each pressure point. Additionally, there is information to be gained from any change in the reflectivity as a function of pressure.

---

[3]Water would be a very interesting material to treat via CMD shock calculations. CMD (static) calculations have been carried out (ref 16) yielding an "effective" intermolecular potential, and that intermolecular potential is available for the CMD shock calculations.

[4]Private conversation.

[5]Since bond breaking requires energy, such an energy loss could be interpreted as a viscous phenomenom.

By taking the derivative of equation 1 with respect to pressure, it can be shown that

$$\frac{\partial R}{\partial p} = 2R^{1/2}(1-R)^{1/2}\left[\frac{(1 \pm \tan^2\theta_f)}{2}\cos\left\{\frac{2\pi}{m_f}\left(\frac{n_o L}{\lambda_o}\right)x\right.\right.$$

$$\left.\left.x\left\{{}_{m_f}\right\}\right\}\right]\frac{\partial m_f}{\partial p} + R^{1/2}(1-R)^{1/2}\int_o^{m_f}(1 \pm \tan^2\theta)x$$

$$x\frac{2\pi}{m_f}\left(\frac{n_o L}{\lambda_o}\right)\left\{\frac{\partial \ln m_f}{\partial p} - \frac{\partial \ln L}{\partial p}\right\}\left\{{}_{m}\right\}\sin\left\{\frac{2\pi}{m_f}\left(\frac{n_o L}{\lambda_o}\right)\left\{{}_{m}\right\}\right\}dm, \quad (8a)$$

where

$$\left\{{}_{m}\right\} \equiv (m+1)^2\sqrt{1-\left(\frac{\sin\theta_o}{m+1}\right)^2} - \cos\theta_o - (\sin^2\theta_o)x$$

$$x\ \ln\frac{(m+1)\left[1 + \sqrt{1-\left(\frac{\sin\theta_o}{m+1}\right)^2}\right]}{1+\cos\theta_o}. \quad (8b)$$

At 5.8 kbar one has, from EOS considerations, $m_f = 0.0405$. For that value of m_f

$$\left\{{}_{m\,=\,0.04}\right\}_{\theta_o\,=\,70^0} \equiv 3.2 \times 10^{-2}.$$

The term in equation 8a containing the derivatives of $\ln m_f$ and $\ln L$ for $(n_o L/\lambda_o) = 10^{-1}$ is smaller[6] by a factor of approximately 0.2 than the first term, which is evaluated at (θ_f, m_f). Thus, there should be sufficient accuracy in the difference between $\frac{\partial R}{\partial p}$ and the first term on the right of equation 8a to determine at least the sign of $\left\{ \frac{\partial \ln m_f}{\partial p} - \frac{\partial \ln L}{\partial p} \right\}$. If hydrogen bond breaking were to lead to a large increase in L with increasing shock pressure, that increase in L would become obvious from sign considerations alone.

SHOCK POLARIZATION CONSIDERATIONS

In this calculation the net orientation of a hydrogen-bonded water, based on the "rigid four-point-charge" model molecule concept (ref 9), is crudely calculated. In the static CMD simulation calculations (ref 19), each four-point-charge molecule interacts via an elecrostatic potential function. Because the calculation presented below considers a single such molecule in an average mechanical force field, the inertial effect of hydrogen bonding is crudely represented by simply placing a hydrogen atom mass at each of the four charge points. See figure 3.

By employing Euler angle transformations (ref 20) and a net z-directed force (due to the shock) on each hydrogen atom, it is possible to derive an equation of motion for θ. Using the Euler angle geometry shown in figure 4 allows θ to be written as

$$m a_{OH} \ddot{\theta} = \frac{2 \ell_o m a_{OH} f_n}{3^{1/2} I_\theta} \sin\theta - \frac{k}{2} \left(\frac{a_{OH}}{a_{HB}} \right)^2 a_{OH} (\delta B_1)^3, \qquad (9)$$

where a_{OH} = oxygen-hydrogen distance ~ 1Å

a_{HB} = hydrogen bonding distance ~ 2Å

---

[6]Because the argument of sine term is small, the total factor to be evaluated is approximately $\left[\frac{2\pi}{m_f} \frac{n_o L}{\lambda_o} \left\{ m_f \right\}^2 \right]$.

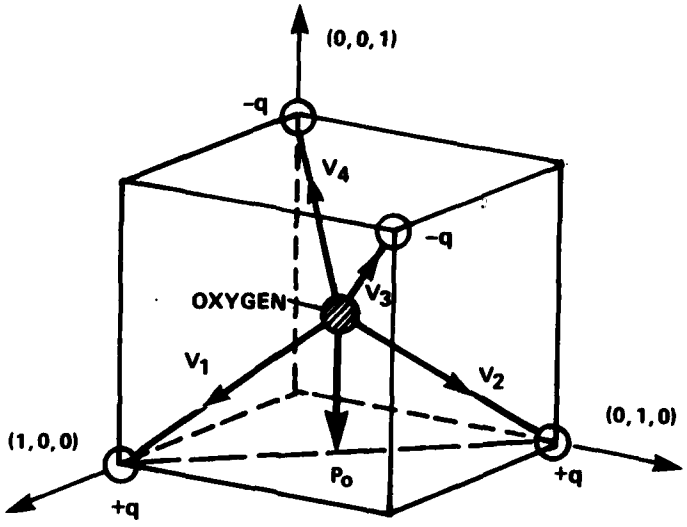

Figure 3. The tetrahedral geometry of the rigid four-point-charge model. P_o is the net molecular polarization, and the $\vec{V}_i$ are the coordinate vectors of the charges (and associated hydrogen masses).

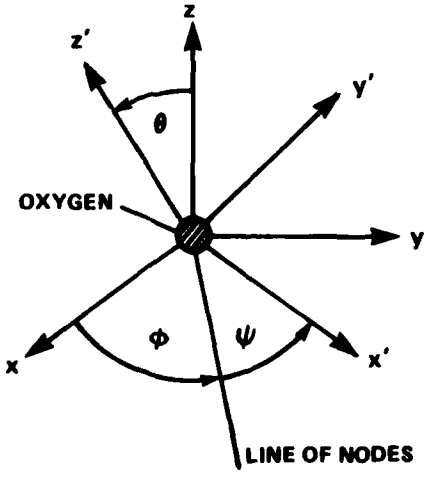

Figure 4. The Euler angle coordinates. The rigid coordinate system attached to the rigid molecule of figure 3 becomes the (x', y', z') system and is allowed to rotate within the fixed system (x, y, z). (θ, ϕ, ψ) are Euler angles.

m = hydrogen atom mass

ℓ_o = $|V_1| - |V_3| = 0.2\text{Å}$

I_θ = moment of inertia about oxygen atom center with respect to line of nodes axis = $\frac{4}{3} m (1.64) (a_{OH})^2$.

f_n = average force on each hydrogen atom = $\alpha \frac{\sigma}{NL_s}$.

k = elastic restoring force coefficient

$\delta\beta_1$ = $\theta - \theta_o$

Equation 9 is the three dimensional version of a calculation first presented by Horie (ref 21). In f_n, α is the fraction of the force per water molecule acting on each hydrogen mass, $\alpha = 1/18$, σ is the shock stress amplitude, N the number density of hydrogen molecules, and L_s is the shock front thickness. It is assumed that f_n acts only within the shock front. The $\delta\beta_1$ term arises from the stretching of the hydrogen bond acting as a restoring force to the angular motion.

The restoring force derivation proceeds with the aid of figure 5 and the assumption of small angle changes, as follows.

$$a_{HB} = a'_{HB} \cos\delta\beta_2 = a'_{HB} \left\{1 - \frac{(\delta\beta_2)^2}{2}\right\}. \tag{10}$$

$$\therefore a'_{HB} - a_{HB} = a_{HB} \frac{(\delta\beta_2)^2}{2}. \tag{11}$$

$$\therefore F = -k(a'_{HB} - a_{HB}) = -k\, a_{HB} \frac{(\delta\beta_2)^2}{2}. \tag{12}$$

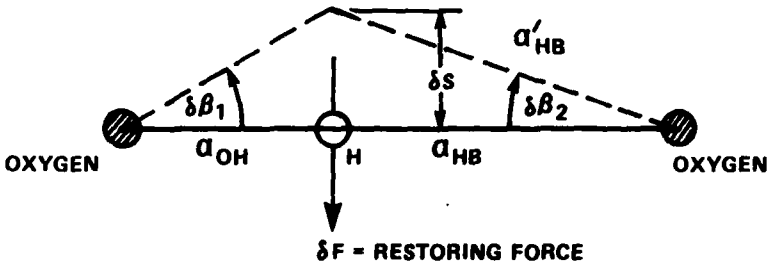

Figure 5. Geometry of the restoring force

$$\delta F = F \sin \delta\beta_2 = - k\, a_{HB} \frac{(\delta\beta_2)^3}{2} . \tag{13}$$

$$\delta F = - \frac{k}{2} \left(\frac{a_{OH}}{a_{HB}} \right)^2 a_{OH} (\delta\beta_1)^3 . \tag{14}$$

Setting $\delta\beta_1 = \theta - \theta_o$, where θ_o denotes the unshocked θ coordinate (thermal motions being neglected) of a particular molecule, is consistent with the crude calculation presented here.

Equation 9 allows two interesting limiting cases: setting $k = 0$ describes the free (bond broken) molecule, or $\ddot{\theta} = 0$ describes the hydrogen bond controlled restoring force limiting angle.

From equation 9 with $\ddot{\theta} = 0$,

$$(\theta - \theta_o)^3 = \frac{16 \ell_o \left(\alpha \frac{\sigma}{NL_s} \right) \sin\theta}{3^{1/2} k \left(\frac{4}{3} a_{OH}^2 \right)} . \tag{15}$$

$$\therefore \theta = \theta_o + \left(\frac{7 \ell_o \alpha \sigma}{k N L_s a_{OH}^2} \right)^{1/3} \sin^{1/3}\theta . \tag{16}$$

With the coefficient of the $\sin^{1/3}\theta$ term assumed small

$$\theta \cong \theta + \left(\frac{7 \ell_o \alpha \sigma}{k N L_s a_{OH}^2} \right)^{1/3} \sin^{1/3}\theta_o , \tag{17}$$

$$\cos\theta \cong \cos\theta_o - \left[\frac{7\ell_o \alpha \sigma}{kNL_s a_{OH}^2}\right]^{1/3} \sin^{4/3}\theta_o. \tag{18}$$

$$\langle\cos\theta\rangle \cong -1/2\left[\frac{7\ell_o \alpha \sigma}{kNL_s a_{OH}^2}\right]^{1/3} \int_o^{\pi} \sin^{7/3}\theta_o d\theta_o, \tag{19}$$

where $\langle\cos\theta\rangle$ denotes the average value obtained by integrating $\cos\theta$ over all possible θ_o positions (on a unit sphere).

Carrying out the integration of equation 19 by simple numerical techniques gives

$$\langle\cos\theta\rangle \cong -(0.74)\left[\frac{7\ell_o \alpha \sigma}{kNL_s a_{OH}^2}\right]^{1/3}. \tag{20}$$

Employing $k = \omega^2 M$, M being the water molecule mass (the rigid water molecule being hydrogen bonded to the surrounding water structure), with ω corresponding to approximately 9 kcal per mole (ref 22), along with $N = 3.47 \times 10^{22}$ cm^{-3}, $\sigma = 10^{10}$ cgs (i.e., 10 kbars), and $L_s = 6.2 \times 10^{-6}$ cm (corresponding to $\beta = 0.2$ in figs 1 and 2) gives

$$\langle\cos\theta\rangle \cong -2.4 \times 10^{-4}. \tag{21}$$

The net shock front produced polarization (in the shock direction) is thus given by

$$\mathcal{P} = -NP_o \langle\cos\theta\rangle, \tag{22}$$

or with $P_o = 2.27 \times 10^{-18}$ esu cm from figure 3,

$$\mathbb{P} = 1.9 \times 10 \text{ cgs}^7 . \tag{23}$$

The weak shock current density at t = 0 (when the shock first enters the water) is given (ref 23) by

$$j_{10} = \frac{\mathbb{P} U}{L_o}, \tag{24}$$

with U being the shock velocity, L_o the water sample thickness, and the subscript 10 denoting 10 kbars. For $U = 2 \times 10^5$ cgs, and $L_o = 1$ cm,

$$j_{10} = 3.8 \times 10^6 \text{ cgs}. \tag{25}$$

Converting to MKS units via $J_{10} = j_{10} / (12\pi \times 10^5)$, and assuming a sample cross section of 10^{-4} m^2, finally gives for the weak shock polarization current in water

$$I_{10} = 10^{-4} \text{ Amperes}. \tag{26}$$

Equation 26 predicts a 10 kbar shock polarization voltage across a 50Ω termination load of 5 mv. Evaluating equations 20 through 24 at 100 kbar with U taken as 5×10^5 cgs (ref 23) and all other parameters unchanged, yields 25 mv for the polarization signal across a 50Ω termination. That 25-mv result is too small by one order of magnitude when compared with the assumed 100-kbar observations of Eichelberger and Hauver (ref 24).

There are a number of possibilities for the small 25-mv result:

1. L_s is approximately two orders of magnitude smaller than the upper limit value of 6.2×10^{-6} cm employed above.

2. The free (i.e. k = 0) molecule version of equation 9 is making at least a partial contribution to $\mathbb{P}$.

---

[7]The actual molecular dipole moment is a complicated function of the hydrogen bonding in liquid water. (See, for example, ref 22.)

3. Little of this section corresponds to reality.

Because the free molecule (i.e., k = 0) version of equation 9 can be shown to yield $\langle\cos\theta\rangle$ results in orders of magnitude larger than those associated with equation 20, the 25-mv calculated value can be seen as supporting the hypothesis that significant bond breaking occurs at pressures approaching 100 kbars. Such bond breaking would add a pressure dependent, free-molecule contribution to $\mathbb{P}$, and would be consistent with ideas put forward by Graham (ref 18).

STATUS SUMMARY

The question of shock front thickness in water remains unanswered except for a predicted upper limit, at 5.8 kbar, of approximately 6×10^{-6} cm. Similarly, the anomalmously large, Soviet shock-related, viscosity values near 100 kbar are neither denied nor confirmed by the theory and experiment reported herein.

Extensive hydrogen bond breaking in liquid water could be an explanation for some guess extrapolations to pressures above 5.8 kbars; however the work carried out to date (October 1981) is insufficient to make a positive judgment on this point.

Hopefully, future theory and experiment outlined in this report will decisively settle all of the outstanding questions.

REFERENCES

1. M. de Icaza-Herrera et al, Revue de Physique Applique, vol 13, (1978), p 547.

2. P. Harris and H. N. Presles, "The Optical Reflectivity of a Shock Front," Technical Report, Laboratoire d'Energetique et de Detonique, University de Poitiers, Poitiers, France, January 1981.

3. P. Harris and H. N. Presles, J. Chem. Phys, vol 74, 1981, p 6864.

4. W. D. Hayes, in Fundamentals of Gas Dynamics, H. W. Emmons, Editor, Princeton University Press, Princeton, NJ, 1958.

5. G. R. Cowan and D. F. Hornig, J. Chem. Phys, vol 18, 1950, p 1008.

6. H. Alsmeyer, J. Fluid Mech, vol 74, 1976, p 497.

7. D. H. Tsai and C. W. Beckett, J. Geophys. Res, vol 71, 1966, p 2601.

8. D. H. Tsai and H. W. Beckett in The Behavior of Dense Media Under High Dynamic Pressure, Symposium, Paris, France, 1967 Gordon and Breach, New York, 1968.

9. K. Niki and S. Ono, Physics Letters, vol 62A, 1977, p 427.

10. W. G. Hoover, Phys. Rev. Letters, vol 42, 1979, p 1531.

11. D. H. Tsai and S. F. Trevino, to be published in Phys. Rev. A.

12. A. Rahman and F. H. Stillinger, J. Chem. Phys, vol 55, 1971, p 3336.

13. O. Weres and S. A. Rice, J. Amer. Chem. Soc, vol 94, 1972, p 8983.

14. O. N. Breusov et al, Soviet Phys. - J.E.T.P., vol 34, 1972, p 591.

15. V. V. Yakushev and A. N. Dremin, "Electrochemical Phenomena in the Shock Compression of Dielectrics," paper given at International Symposium on Explosives, Cladding, 1st, 1970 (1971). Translation appears as report SAND80-6005, Sandia National Laboratories, Albuquerque, NM, 1980.

16. A. Rahman and F. H. Stillinger, J. Chem. Phys, vol 55, 1971, p 3336.

17. S. D. Hamann in Proceedings of the 1979 Nobel Berzelius Symposium on "Chemistry and Geochemistry of Solutions at High Temperature and Pressure," Pergamon, 1981.

18. R. A. Graham, J. Phys. Chem, vol 83, 1979, p 3048.

19. F. H. Stillinger and A. Rahman, J. Chem. Phys, vol 60, 1974, p 1545.

20. H. Goldstein, Classical Mechanics, Addison-Wesley, Cambridge, MA, 1950.

21. Y. Horie, J. Phys. D, vol 1, 1968, p 1183.

22. A. Goel et al, Indian J. Chem, vol 9, 1971, p 56.

23. M. H. Rice and J. M. Walsh, J. Chem. Phys, vol 26, 1957, p 824.

24. R. J. Eichelberger and G. E. Hauver, in Les Ondes des Detonations, Centre Nationale de la Recherche Scientifique, Paris, 1962.

DISTRIBUTION

Commander
U.S. Army ARRADCOM
ATTN: DRDAR-TD, Dr. R. E. Weigle
DRDAR-TSS (5)
DRDAR-LC, Dr. J. Frasier
DRDAR-LCN, Mr. H. Grundler
Dr. P. Harris (50)
DRDAR-LCA, Mr. W. Benson
Dr. Harry Fair
Dr. T. Gora
Mr. W. Doremus
Dr. G. Vezzolli
DRDAR-LCE, Dr. R. Walker
Mr. Louis Avrami
Dr. F. Owens
Dr. C. Capellos
DRDAR-GCL
Dover, NJ 07801

Director
Lawrence National Laboratory
ATTN: Dr. Frank E. Walker
Dr. A. M. Karo
Livermore, CA 94550

Stanford Research Institute
Poulter Laboratories
ATTN: Dr. William J. Murri
Dr. D. R. Curran
Dr. R. K. Linde
Menlo Park, CA 94025

Sandia National Laboratory
ATTN: Dr. Walter Hermann
Dr. Robert Graham
Dr. D. B. Hayes
Dr. J. Gover
Dr. William Benedick
Dr. R. E. Hollenbach
Dr. L. D. Bertholf
P.O. Box 5800
Albuquerque, NM 87116

Washington State University
ATTN: Dr. George Duvall
Dr. G. R. Fowles
Dr. George Swan
Pullman, WA 99163

Commander
U.S. Naval Surface Weapons Center
Explosion Dynamics Division
ATTN: Dr. D. John Pastine
Dr. S. J. Jacobs
Dr. J. Forbes
Dr. James Goff
White Oak, MD 20910

Commander
U.S. Army Research Office
ATTN: Dr. J. Chandra
Dr. C. Boghosian
Dr. I. Lefkowitz
P.O. Box 12211
Research Triangle Park, NC 27709

Commander
U.S. Army Research and Standardization
Group (Europe)
P.O. Box 65
FPO 09510

National Bureau of Standards
ATTN: Dr. Donald Tsai
Dr. Henry Prask
Gaithersburg, MD 20760

California Institute of Technology
ATTN: Dr. Thomas J. Ahrens
Dr. Lien G. Yang
Pasadena, CA 91109

Department of Chemistry and
Chemical Engineering
ATTN: Dr. H. G. Drickamer
Urbana, IL 60436

Commander
ARRADCOM
Ballistic Research Laboratories
ATTN: Dr. Philip Howe
Dr. Donald Eccleshall
Dr. George Adams
Dr. Robert F. Eichelberger
Dr. George E. Hauver
Dr. D. F. Strenzwilk
Dr. Y. K. Huang
Dr. I. May
DRDAR-TSB-S (Tech Library)
Aberdeen Proving Ground, MD 21005

Commander
Benet Weapons Laboratory, LCWSL
ATTN: Dr. T. E. Davidson
DRDAR-LCB-TL (Tech Library)
Watervliet, NY 21289

University of Delaware
Department of Physics
ATTN: Prof. Ferd E. Williams
Prof. W. B. Daniels
Newark, DE 19711

Director
Defense Technical Information Center
ATTN: Accessions Division (12)
Cameron Station
Alexandria, VA 22314

Union Carbide Corporation
Tarrytown Technical Center
ATTN: Dr. Jaak Van Den Sype
Tarrytown, NY 10591

McDonnel Douglas Astronautics
ATTN: Dr. John Watcher
Dr. Harvey Berkowitz
5301 Bolsa Ave
Huntington Beach, CA 92647

Systems, Science, and Software
ATTN: Dr. H. E. Read
P.O. Box 1620
La Jolla, CA 92037

Director
Defense Nuclear Agency
Washington, DC 20305

Army Materials & Mechanics Center
ATTN: Mr. John F. Dignam
Mr. John Mescall
Dr. D. P. Dandekar
Building 131
Arsenal Street
Watertown, MA 02172

Lockheed Palo Alto Research Labs
ATTN: Dr. J. F. Riley
3251 Hanover Street
Palo Alto, CA 94304

Bell Telephone Laboratories
ATTN: Dr. F. H. Stillinger
Murray Hill, NJ 07974

Director
Los Alamos Scientific Laboratory
ATTN: Dr. J. M. Walsh
Los Alamos, NM 87544

Commander
U.S. Army Missile Research and
Development Command
ATTN: Dr. Charles M. Bowden
Redstone Arsenal, AL 35809

University of Tennessee
ATTN: Prof. M. A. Breazeale
Dept of Physics and Astronomy
Knoxville, TN 37916

Princeton University
ATTN: Prof. A. C. Eringen
Princeton, NJ 08540

Carnegie Mellon Institute
of Technology
ATTN: Prof Morton E. Gurtin
Dr. Bernard D. Coleman
Department of Mathematics
Pittsburgh, PA 15213

Brown University
ATTN: Prof Robert T. Beyer
Department of Physics
Providence, RI 02912

Courant Institute of
Mathematical Sciences
ATTN: Library
New York University
New York, NY 10453

City College of the
City University of New York
ATTN: Prof Harry Soodak
Department of Physics
139th Street & Convent Ave
New York, NY 10031

Queens College of the
City University of New York
ATTN: Prof Arthur Paskin
Department of Physics
Flushing, NY 11300

SPIRE Corp
ATTN: Dr. Roger Little
Patriots Park
Redford, MA 01730

Director
U.S. Army Materiel Systems
Analysis Activity
ATTN: DRXSY-MP
Aberdeen Proving Ground, MD 21005

Commander/Director
Chemical Systems Laboratory
U.S. Army Armament Research
and Development Command
ATTN: DRDAR-CLJ-L
DRDAR-CLB-PA
APG, Edgewood Area, MD 21010

Commander
U.S. Army Armament Materiel
Readiness Command
ATTN: DRSAR-LEP-L
Rock Island, IL 61299

Director
U.S. Army TRADOC Systems
Analysis Activity
ATTN: ATAA-SL
White Sands Missile Range, NM 88002

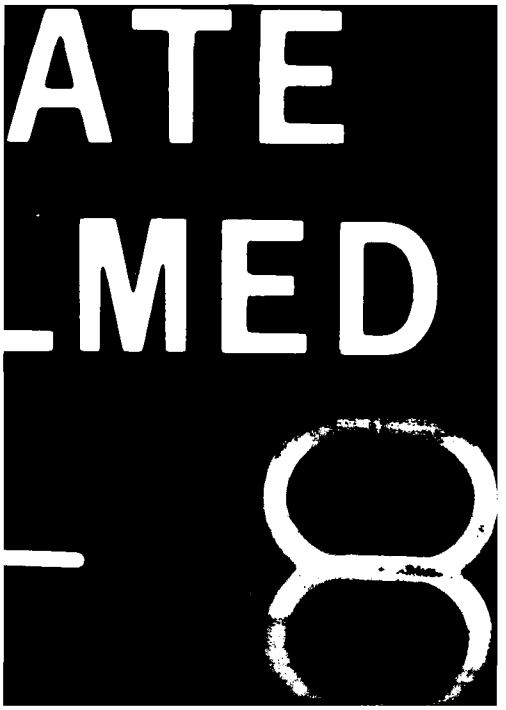
ATE
LMED
8